A Wideband Noise-like Transmitter Approach for Underwater Lidar using Diode Lasers and Passive Fiber Optic Processors

Luke K. Rumbaugh, David W. Illig,
Mahesh K. Banavar, and William D. Jemison
Department of Electrical and Computer Engineering
Clarkson University, Potsdam, New York
rumbaulk@clarkson.edu

Brandon Cochenour
Electro-Optic and Special Mission Sensors Division
Naval Air Warfare Center
Patuxent River, Maryland

***Abstract*—A new wideband noise-like transmitter approach is presented for high resolution underwater lidar sensing. The transmitter approach is based on small-footprint, low-cost components, using low coherence time laser diodes and passive fiber processors to generate wideband noise-like intensity modulation signals in the blue-green optical spectrum. Prototype transmitters are demonstrated using both blue and green laser diodes with passive fiber interferometer structures. Laboratory water tank experiments using a two-diode 516/518 nm prototype transmitter show centimeter range error and 30 cm range resolution while detecting a submerged gray target in up to ten attenuation lengths of turbid water. Experimentally observed challenges for target rangefinding are discussed, including shot noise, backscatter returns, and self-clutter. Strategies are proposed to mitigate these challenges and enhance performance when operating at long standoff distances in turbid waters.**

I. Introduction

Underwater lidar sensors can provide high range and spatial resolution in ranging and imaging applications [1]–[4]. However, the absorption and scattering of light underwater present challenges to these sensors, especially in highly turbid waters [5]–[7]. Absorption and scatter can cause performance degradation by decreasing the power in the desired reflection signals, while backscatter can cause false alarms and increase receiver shot noise. Blue and green lasers are typically used to minimize absorption, and one means of suppressing backscatter is the use of wideband intensity modulation signals. Wideband lidar supports discrimination of desired object reflection signals from undesired backscatter signals both in the frequency domain, where the backscatter return decorrelates at high intensity modulation frequencies [8], [9], and in the temporal (range) domain, where object returns and backscatter returns appear as distinct peaks [10]–[13].

One recently introduced blue-green wideband lidar technique is noise-like lidar. Noise-like radar and lidar sensors use wide bandwidth transmitters and cross-correlating receivers to produce returns with high temporal resolution and high sensitivity [14]–[16]. The large time-bandwidth products of their wideband waveforms provide signal-to-noise ratio enhancement via pulse compression gain, and the matched filter receivers give near-optimal noise rejection. A blue-green underwater noise-like lidar sensor has recently been implemented that uses wideband chaotic intensity modulation for high resolution rangefinding and impulse response measurements [13], [17]. This sensor uses a transmitter based on near-infrared fiber laser and fiber amplifiers, an approach that allows high signal bandwidth and power to be generated in the infrared [3], [12], [18]. The transmitter uses an optical frequency doubler to generate a modulated blue-green signal useful for underwater work.

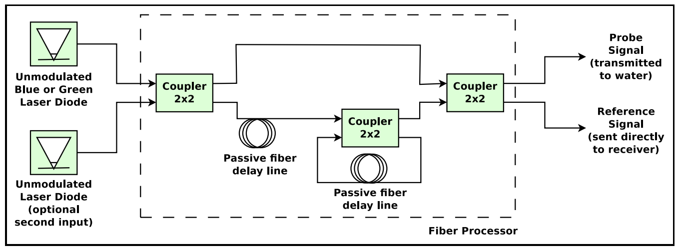

Fig. 1. This paper introduces a noise-like transmitter architecture for underwater lidar. The proposed transmitter approach uses a low coherence time blue or green laser diode, with a passive fiber processor to introduce wideband intensity modulation.

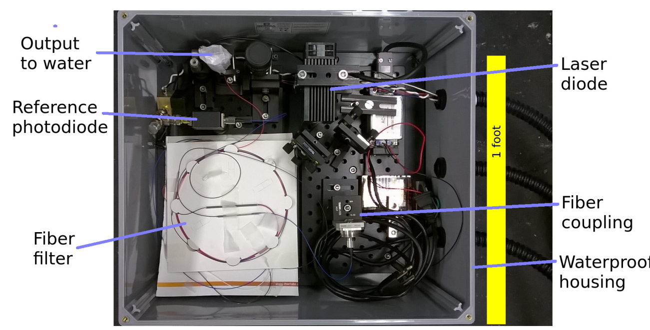

Fig. 2. Several prototype transmitters have been constructed at various wavelengths. The transmitter pictured uses a 442 nm diode and sits in a 16”x14”x7” waterproof enclosure.

This paper introduces a new approach to noise-like intensity modulation signal generation for underwater lidar. This transmitter approach, shown conceptually in Figure 1 and in a prototype in Figure 2, uses blue or green laser diodes and passive fiber optic processors to generate wide bandwidth noise-like intensity modulation signals directly in the desired blue-green spectrum. No electrical signal generator, active modulator, or frequency doubler are used. This approach allows use of low cost, commercially available components in a transmitter with a small size, weight, and power footprint.

978-0-933957-43-5

These advantages should increase the compatibility of noise-like lidar sensors with packaging and deployment aboard small and mobile platforms. Since the fiber processors used are compatible with any low coherence time blue or green laser source, the transmitter wavelength can be changed by replacing the diode or tuning its wavelength, and multiple wavelength approaches can be explored. The output power can also be scaled by using multiple input diodes. Because the transmitter approach is wideband and nonlinear, it should also be compatible with previously proposed calibration routines [13] and several signal processing techniques such as frequency domain filtering [8], [19], blind signal separation [20], and nonlinear processing [21].

In this paper, the proposed transmitter approach is demonstrated for the first time, using a blue prototype operating at 442 nm, and a green prototype using two diodes operating at 516 nm and 518 nm. Section II describes the prototypes and shows their wideband intensity modulation signals. Section III describes proof of concept underwater experiments in which the two-diode 516/518 nm prototype was used to range a submerged target in a laboratory water tank. Several challenges for underwater rangefinding using this approach are observed in the experimental results. Section IV proposes mitigation strategies for these challenges, including a calibration routine, modulation depth enhancement, and several signal processing techniques. Section V provides conclusions and proposed future work.

II. Noise-like Transmitter

Figure 1 shows the noise-like transmitter approach, which uses an unmodulated blue or green laser diode as a light source. The laser signal is coupled into a fiber interferometer, which converts the phase noise of the diode into intensity noise modulation. An advantage of this approach is that it allows use of low-cost, commercially available blue and green laser diodes recently developed for mass market display applications. Such diodes typically have low coherence times associated with broadband phase noise. While this phase noise is undesirable for many applications, it can be converted to wideband intensity noise with advantages for lidar by using fiber interferometers [22]. The single-mode fiber interferometer used in the proposed approach is a resonator-enhanced Mach Zehnder interferometer (REMZI), which offers high sensitivity to phase changes [23]. The stability of the interferometer against environmental perturbation is ensured by use of a long delay in the resonator loop [24], [25]. The two outputs of the interferometer have a cross-correlation function that approximates a thumbtack, allowing one output of the interferometer to be used as the probe signal transmitted to the water, and the other to be held as a reference signal. The reference signal can then be used as a matched filter for the probe signal returning from reflective particles and objects in the water.

Two prototype transmitters were constructed for proof of concept of this transmitter approach. The first prototype is shown in Figure 2. It uses a low-cost 442 nm multimode laser

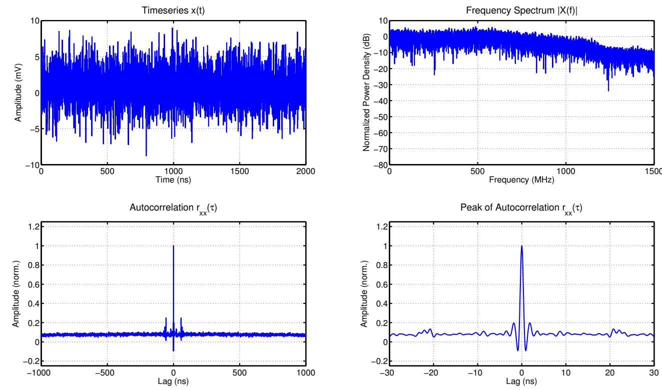

Fig. 3. Noise-like intensity modulation signal generated by a prototype transmitter using a 442 nm laser diode. Top left: Time domain, showing noise-like intensity modulation. Top right: Power spectral density, showing >1 GHz bandwidth. Bottom left: The autocorrelation function approximates a thumbtack, with no periodicity. Bottom right: The main peak of the autocorrelation function has a 3 dB peak width of 0.6 ns.

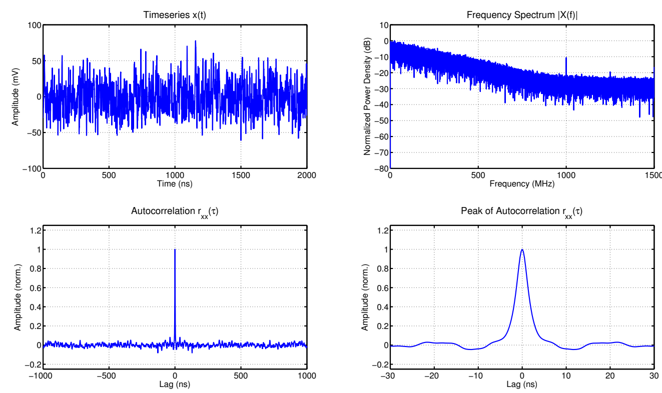

Fig. 4. Noise-like intensity modulation signal generated by a prototype transmitter using both 516 nm and 518 nm laser diodes. Top left: Time domain, showing noise-like intensity modulation. Top right: Power spectral density, showing a monotonically decreasing spectrum from DC to 1 GHz. Bottom left: The autocorrelation function approximates a thumbtack, with no periodicity. Bottom right: The main peak of the autocorrelation function has a 3 dB peak width of 3 ns.

diode (Aixiz AIX-445-A) with a 10-m delay in the single-mode fiber REMZI. The REMZI uses three 1x2 488 nm 3.5 μm couplers (Haphit FICL-488-50-1), one 2x2 488 nm coupler (Thorlabs FC488-50B-FC), and 3.5 μm passive visible light fiber (Nufern 460HP) throughout. The output power of the 442 nm prototype is 250 μW, as limited by the efficiency of launching this multimode diode beam into the single-mode 3.5 μm fiber core. Figure 3 shows the intensity modulation signal generated by this transmitter. The output signal is noise-like, with power distributed over the spectrum from DC to >1 GHz. The cross-correlation of the fiber outputs is an impulse with 0.60 ns 3 dB peak width, sidelobes at 6 dB below the main peak, some additional spurious self-clutter elements, and no periodicity.

A second transmitter prototype uses a fiber-coupled single-mode 516 nm laser diode (Thorlabs LP520-SF15) and 25 m single-mode fiber REMZI. The REMZI uses three 2x2 532 nm couplers (Thorlabs FC532-50B-FC) and 3.5 μm passive fiber (Nufern 460HP) for pigtails and delays. The measured output power at the output fiber tip of the 516 nm fiber-coupled diode was 14 mW, and 4 mW was measured at each output of the interferometer. Thus the gross optical efficiency through the interferometer is estimated at 50-60%, with half of the output light available for transmission into the water. The power was scaled by coupling a second fiber-coupled diode to the second input port of the interferometer: adding a 518 nm diode (Thorlabs LP520-SF15) with 14 mW output power produced 8 mW at each output of the interferometer. (A 518 nm diode was used to avoid spectral overlap with the 516 nm diode, so that independent interference patterns would be generated at each wavelength.) Figure 4 shows the intensity modulation signal generated by the transmitter using both the 516 nm and the 518 nm diodes. The output signal is noise-like, with frequency content from DC to 1 GHz. The cross-correlation of the outputs had a 3 ns 3 dB peak width, sidelobes 11 dB down from the peak, some additional self-clutter elements, and no periodicity. The wider peak width for the 516 nm cross-correlation is due to its reduced intensity modulation bandwidth relative to that of the 442 nm transmitter. This is thought to be due to a lower phase noise bandwidth in the 516 nm and 518 nm single-mode diodes compared to the 442 nm multimode diode.

The modulation depth of the 516/518 nm prototype's signal is approximately 0.5, so that the modulated signal power transmitted into the water is about 4 mW. Taking the bandwidth as 333 MHz (from the 3 ns peak width of the autocorrelation) and hypothesizing a 10 μs dwell time, the time bandwidth product will be on the order of 3330, for a post-correlation energy per measurement of 13.33 μJ. This suggests rangefinding performance might become absorption-limited at about 13 attenuation lengths downrange for an ideal receiver [4] (although the modulation depth of 0.5 implies that this estimate should be corrected downward by 3 dB, or by 0.35 downrange attenuation lengths). The noise-like signal's autocorrelation has self-clutter sidelobes about 11 dB below the main peak, implying that target rangefinding in turbid water may also become scatter-limited in turbid water, if the target-to-backscatter-peak ratio falls below -11 dB. In this case, the self-clutter sidelobes from the backscatter signal might obscure the target peak.

III. Underwater Measurements

Underwater measurements were demonstrated in a laboratory test tank. Figures 5 and 6 show the experimental setup. The 516/518 nm prototype transmitter generated a noise-like intensity modulation signal, with the 516 nm and the 518 nm diodes operating simultaneously. One output of the fiber interferometer's 2x2 output coupler was detected by a fiber-coupled photodetector (Thorlabs DET025AFC) and held as a reference signal. The beam from the other output was transmitted into the water as a probe signal, with 6 mW optical power entering the water. The reflection from a submerged gray test target was detected by a photomultiplier tube (PMT) with a 50 mm aperture and 10^4 gain (Photonis 5-stage). The output of the PMT was AC-coupled using a bias tee (Minicircuits ZFBT-4R2GW) to remove unmodulated signal and decorrelated

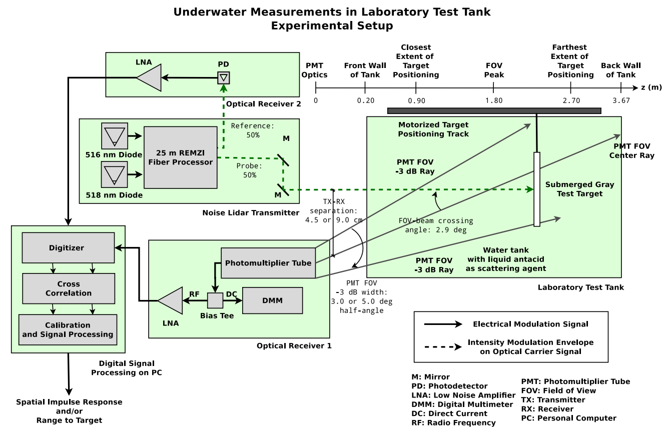

Fig. 5. Experimental setup for underwater measurements using the 516/518 nm noise-like transmitter prototype. This setup in a laboratory test tank was used to demonstrate rangefinding to a gray target submerged in turbid water.

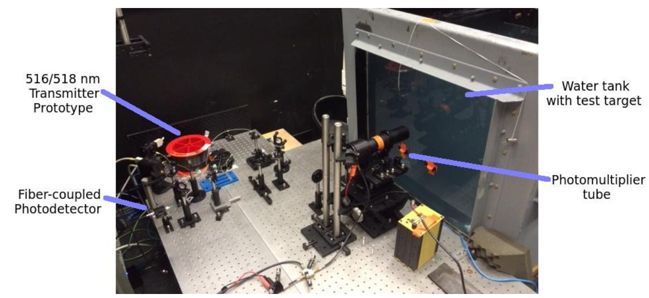

Fig. 6. Photograph of the underwater measurement experimental setup, showing the 516/518 nm noise-like transmitter, the two optical receivers, and the laboratory test tank.

backscatter; the AC signal was then amplified by a 20 dB 10-1000 MHz amplifier (Minicircuits ZFL-1000VH). Both the amplified AC signal from the PMT and the DC-coupled signal from the photodetector were then digitized by a 12-bit analog/digital converter (ADC) running at 4 gigasamples/sec (SP Devices ADQ412DC-4G). A computer was used for digital signal processing. The reference and probe signals were each collected in synchronized 8.75 μs (35 kilosample) segments, and each pair of segments were windowed and cross-correlated to obtain a single lidar return. Converting cross-correlation delay time to downrange distance, each return provided an estimate of the 1-axis downrange spatial impulse response of the channel (i.e. the temporal impulse response times the speed of light, divided by two to account for the light's round-trip back to the sensor).

A. Rangefinding

Proof of concept rangefinding was performed by varying the test target location and the water turbidity. Measurements were taken repeatedly as the target was moved from 0.9 m to 2.7 m downrange of the sensor by a motorized cart traveling at 4 cm/sec. The perpendicular distance between the laser beam and the center of the PMT collection lens was 9 cm, and the PMT field of view (FOV) was 3.4° half-angle. The turbidity was varied by adding Equate liquid antacid to the tank, and was monitored by the 510 nm sensor of a spectrophotometer (Wetlabs AC-9).

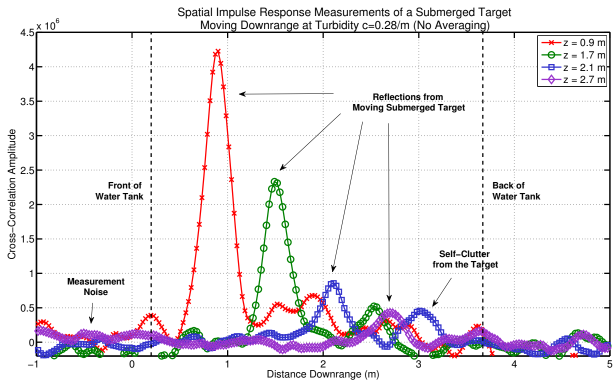

Fig. 7. Experimental spatial impulse response returns obtained for a gray test target submerged in water with extinction coefficient c=0.28/m. Each return corresponds to a different target position. As the target is moved downrange, the amplitude of its reflection peak in the returns shifts downrange and falls in amplitude. Shot noise is visible, as well as spurious self-clutter artifacts that scale with the target peak.

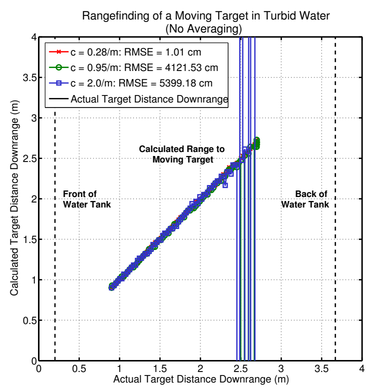

Fig. 8. Experimental demonstration of rangefinding to a gray test target submerged in turbid water and moved continuously from 0.9 m to 2.7 m downrange of the lidar sensor. Each data set corresponds to a different water turbidity. Using a single return of dwell time of 8.75 μs, target detection breaks down after 2 m (or, four attenuation lengths).

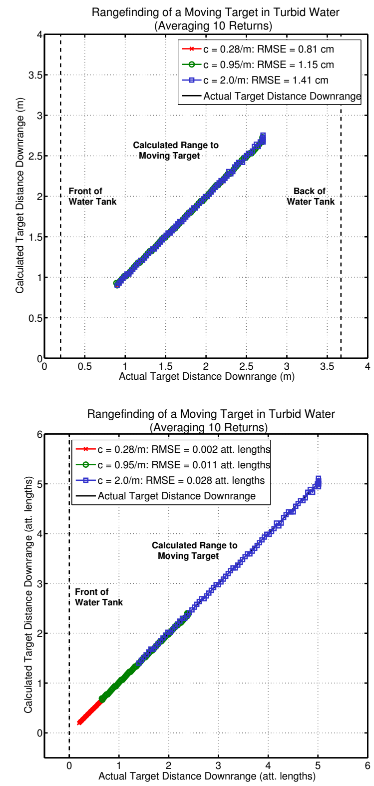

Fig. 9. Experimental demonstration of rangefinding to a gray test target submerged in turbid water and moved continuously from 0.9 m to 2.7 m downrange of the lidar sensor. Each data set corresponds to a different water turbidity. Top: Averaging 10 lidar returns to suppress shot noise, ranging performance is maintained to the end of the measurement track with a root mean squared error (RMSE) on the order of 1 cm. Bottom: The same range calculations, plotted against attenuation lengths. Accurate ranging continues past five attenuation lengths.

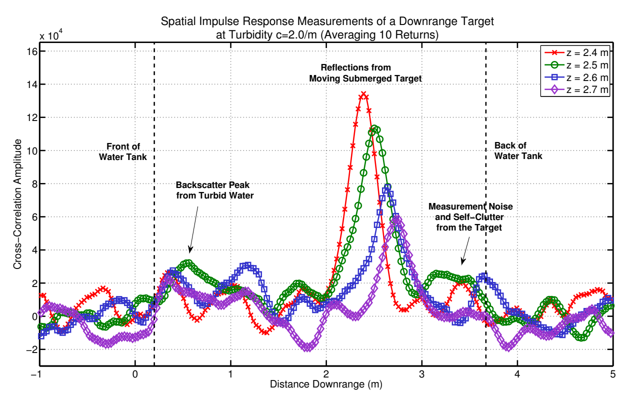

Fig. 10. Experimental spatial impulse response measurements taken at turbidity c=2.0/m and averaging ten returns, showing target positions near five attenuation lengths downrange from the sensor. Shot noise is becoming strong, and a backscatter peak from the turbid water is seen, suggesting that breakdown would occur in the next few attenuation lengths. Self-clutter from the peak is also visible.

Figure 7 shows sample measurements obtained while the target was moving downrange in water with a 510 nm extinction coefficient of c=0.28/m. (Here, c is the exponential attenuation coefficient per meter.) The target's downrange movement is reflected in the changing peak locations in the lidar returns, while the peak amplitude falls off exponentially with distance due to the attenuation of the water. The 3 dB range resolution of the target peaks is about 30 cm, corresponding to the autocorrelation peak width of the 516/518 nm transmitter prototype's intensity modulation. Measurement noise and self-clutter begin to obscure the target return at the farthest distance shown. The measurement noise was experimentally determined to be primarily shot noise. The self-clutter associated with each target peak retains a consistent shape, and is scaled by the amplitude of the target peak.

For rangefinding, the highest peak in the lidar return was treated as the object of interest, and its downrange distance was reported. Figure 8 shows the measured distance to the highest peak in the lidar return versus the actual position of the test target as it was moved downrange, for several water turbidities. When a single 8.75 μs return was used for each range calculation, shot noise obscured the target for longer target distances and higher turbidities. By averaging ten returns for each measurement, for a total measurement dwell time of 87.5 μs, ranging was maintained along the entire track, as shown in Figure 9, with a root mean squared error (RMSE) on the order of 1 cm. The target position is also

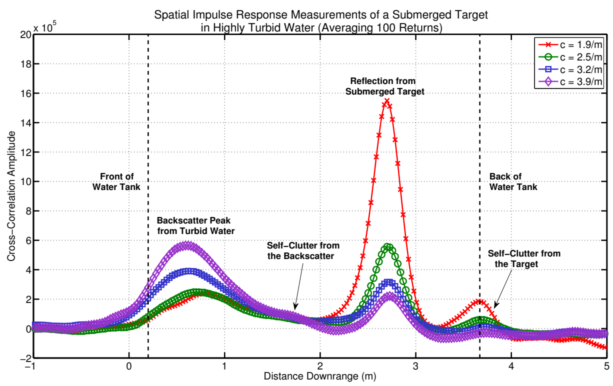

Fig. 11. Experimental spatial impulse response measurements taken in several high turbidity water conditions, averaging 100 lidar returns to suppress shot noise and highlight the effects of the backscatter. As the turbidity increases, the amplitude of the reflection from the target decreases, and the amplitude of the backscatter peak increases and sharpens. The self-clutter sidelobes associated with the backscatter peak also grow with turbidity.

shown in terms of attenuation lengths (where an attenuation length is the downrange distance traveled in water, times the water's extinction coefficient), showing performance past five attenuation lengths. Figure 10 shows the averaged spatial impulse response measurements seen near five attenuation lengths: the shot noise is within a few dB of the target peak, and the backscatter peak is increasing. Self-clutter is again visible near the target.

B. High Turbidity Spatial Impulse Response Measurements

In order to further investigate the effects of the backscatter at high attenuation lengths, measurements were taken of the target at 2.7 m downrange at turbidities ranging from c=1.9/m to c=3.9/m. To isolate the backscatter effects from shot noise effects, 100 lidar returns were averaged. The viewing geometry was also increased to admit more backscatter by reducing the perpendicular distance between the beam and the PMT lens center to 4.5 cm and increasing the PMT FOV to 5.8° half-angle. The resulting measurements are shown in Figure 11. As the turbidity increased, the backscatter peaks sharpened, moved towards the lidar system, and increased in amplitude, while the target peaks decreased in amplitude, so that at the highest turbidity the backscatter peak was larger than the target peak. Self-clutter associated with the backscatter peak also grew to within a few dB of the target peak. The target peak remained visible in all cases, including the last where the target was 9.8 attenuation lengths downrange of the sensor.

C. Discussion: Lidar Performance Challenges

The experimental results shown in Figures 7-11 indicates that while this transmitter prototype can give accurate range measurements at several attenuation lengths, challenges can be expected as turbidity and target distance are increased. The shot noise forced the use of averaging after a few attenuation lengths. Averaging ten returns allowed accurate ranging to five attenuation lengths as shown in Figure 9. At this point, the shot noise was again significant and the backscatter peak also became evident, as shown in Figure 10, such that breakdown

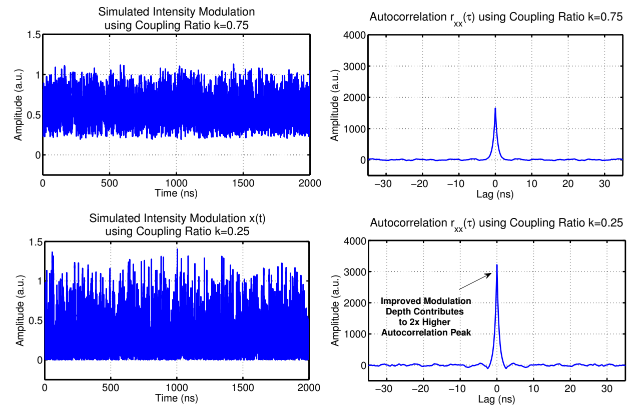

Fig. 12. Modulation depth improvement by changing the transmitter fiber parameters is under investigation. Top left: Simulation of a REMZI transmitter, showing a partially modulated output signal when fiber coupling ratios of k=0.75 are used at the REMZI input and output couplers. Top right: The autocorrelation peak of the partially modulated signal. Bottom left: When k=0.25 is used, the simulated output signal becomes fully modulated. Bottom right: The energy in the autocorrelation peak is increased by a factor of two. If implemented, such an improvement would double the achievable signal-to-shot-noise-ratio and allow operation at shorter measurement dwell times.

can be expected within a few more attenuation lengths. By further increasing averaging to 100 returns, the shot noise was suppressed, allowing target detection out to ten attenuation lengths, as shown in Figure 11. Here, the backscatter effects were strongly visible, challenging target ranging in two ways. First, as the turbidity increased, the backscatter peak in the measurement became sharper, and discrimination of the target peak from the backscatter peak became less certain. Second, when the backscatter peaks were strong, self-clutter sidelobes due to the backscatter begin to emerge, which could obscure small reflections from the target. Thus while the target was still detected at ten attenuation lengths, it would likely be lost in the backscatter's self-clutter within a few more attenuation lengths.

The next section presents strategies that may help mitigate these experimentally observed challenges.

IV. Addressing Lidar Performance Challenges

The three challenges noted in the underwater proof of concept experiments were low signal-to-shot-noise-ratio (SSNR), high backscatter peaks, and spurious self-clutter. This section discusses possible mitigation strategies. The SSNR can be improved by increasing dwell time if feasible, and by improving the transmit signal's modulation depth. Suppression of the backscatter peak in turbid waters can be done using frequency domain filtering as discussed below, and also by blind signal separation as discussed in [20]. Spurious self-clutter sidelobes can be mitigated by application of a calibration routine or by use of nonlinear processing. Both of these techniques can remove spurious artifacts caused by the transmitter and receiver hardware.

A. Increasing Signal-to-Shot-Noise-Ratio: Modulation Depth Enhancement

Since the receiver shot noise depends on the mean total optical intensity seen by the PMT, unmodulated light received by the PMT should be minimized, if possible. Such unmodulated light contributes to the shot noise, but not to the lidar measurement. In the underwater experiments performed, both the decorrelated backscatter signal and the reflected unmodulated transmit signal were sources of shot noise. While the backscatter decorrelation is acceptable and helpful in target detection, having any unmodulated component of the transmit signal is undesirable, and suggests that improvement of the modulation depth of the transmit signal should improve system performance at low measurement dwell times.

The modulation depth of the transmitted signal depends on the parameter values selected for the fiber REMZI. The modulation depth is especially sensitive to the coupling ratios used in the REMZI couplers. Figure 12 shows simulated noise-like modulation signals for two values of the input and coupling ratios. When the intensity coupling ratios are 0.75, the simulated intensity modulation signal is partially modulated, with a strong DC offset. When the ratios are changed to 0.25, the signal is fully modulated. The corresponding autocorrelation peak amplitude is double that of the partially modulated signal. When used underwater, the SSNR would likewise be doubled. Modulation depth improvement by changing the transmitter prototypes' coupling ratios is currently under investigation.

B. Reducing Backscatter Peaks: Frequency Domain Filtering

Modulation depth of optical backscatter has been shown to decrease monotonically with increasing intensity modulation frequency [9]. In the experimental setup in Figure 5, decorrelated (unmodulated) backscatter is removed from the lidar measurement using a bias tee. The remaining modulated backscatter resides primarily in the lower ranges of the frequency spectrum, with a frequency response that depends on the turbidity of the water, but is in general low-pass. Meanwhile the target's broad frequency response returns a frequency spectrum similar to that of the transmitted noise-like signal, which for the 516/518 nm prototype had frequency content out to 1 GHz. As shown in Figure 13, application of a high-pass frequency domain filter allows suppression of the backscatter component found at low frequencies, while maintaining the target component's high frequency content. Figure 14 shows the application of a bandpass filter to the four underwater lidar measurements shown in Figure 11. The filter selected is a 33-tap linear-phase finite impulse response (FIR) filter with a 185 MHz lower 3-dB cutoff frequency and an 890 MHz 3-dB upper cutoff frequency. (The upper cutoff of the bandpass filter helps with high frequency noise rejection.) The filtered lidar measurements show strong suppression of the backscatter return, isolating the target return. Such processing could increase the probability of detection when operating in turbid water.

C. Removing Self-Clutter: Calibration and Nonlinear Processing

The spurious self-clutter artifacts seen in the lidar returns cannot be mitigated by averaging or signal energy increase. They are due to hardware imperfections in the transmitter and

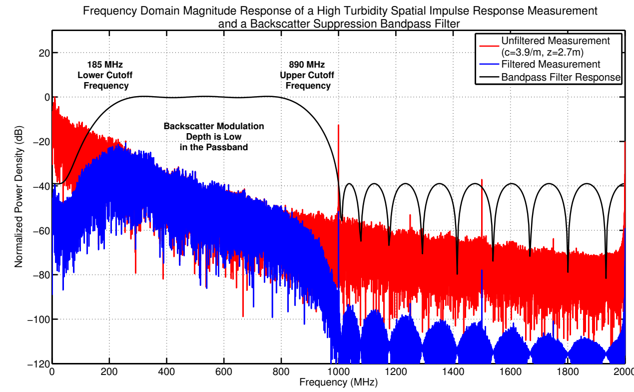

Fig. 13. Frequency domain magnitude responses of the highest turbidity spatial impulse response from Figure 11, and the 185-890 MHz bandpass linear-phase finite impulse response (FIR) filter used to suppress the backscatter.

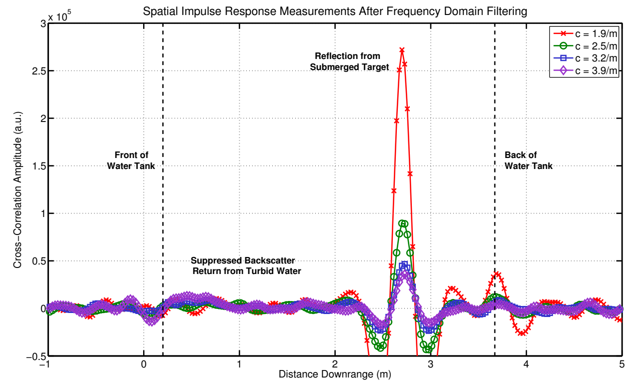

Fig. 14. The FIR filter of Figure 13 is applied to the high-turbidity spatial impulse response measurements of Figure 11. The backscatter return is suppressed and the target return is isolated.

in the receiver. The noise-like transmit signals generated by the transmitter prototypes have autocorrelation functions that approximate thumbtacks, but these autocorrelation functions do have undesired self-clutter structures. The underwater lidar sensor configuration shown in Figure 5 also has mismatched receivers: in this arrangement, a large-aperture PMT is used as "Optical Receiver 1" and a fiber-coupled photodiode is used as "Optical Receiver 2".

To mitigate the effect of spurious sensor hardware artifacts in the measurements, an experimental calibration routine can be used [13]. This routine uses a free-space or clear-water measurement to characterize the receiver mismatch. Then, the transmit signal's autocorrelation is estimated concurrently with each underwater profile measurement. The receiver mismatch and the transmitter autocorrelation are then deconvolved from the raw lidar measurement, removing the self-clutter and isolating the desired spatial impulse response of the underwater scene itself. Figure 15 shows several raw lidar measurements with significant self-clutter, and Figure 16 shows the removal of self-clutter achieved by applying this calibration routine to these measurements. The uncalibrated measurements include several spurious artifacts arising both from the transmit signal and the receivers, for example the slow rise time on the target peaks, and the secondary peak about 7 dB lower than, and

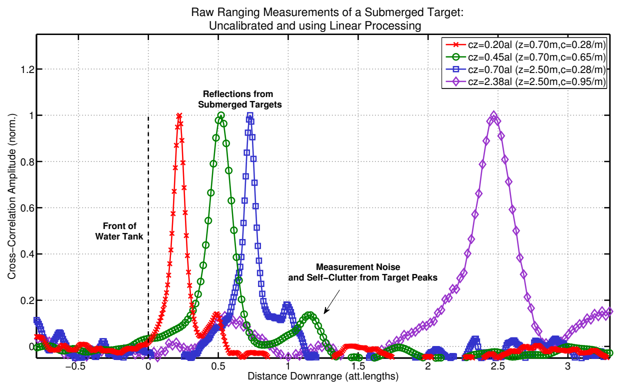

Fig. 15. Spurious self-clutter artifacts due to the transmitter and receiver hardware were observed in the experimental measurements. Here, four raw ranging measurements are shown, which have strong self-clutter elements.

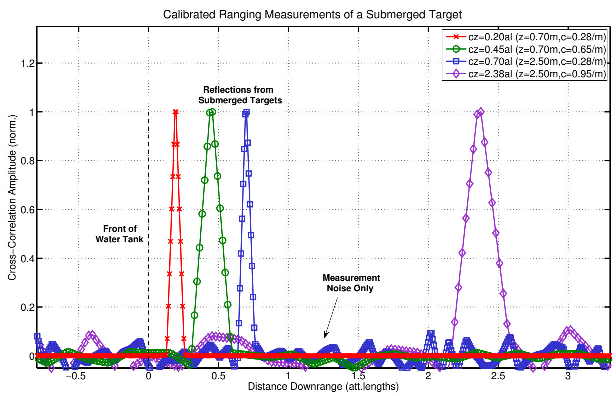

Fig. 16. After applying a calibration routine, the self-clutter artifacts in the four raw ranging measurements from Figure 15 have been removed, and only measurement noise remains.

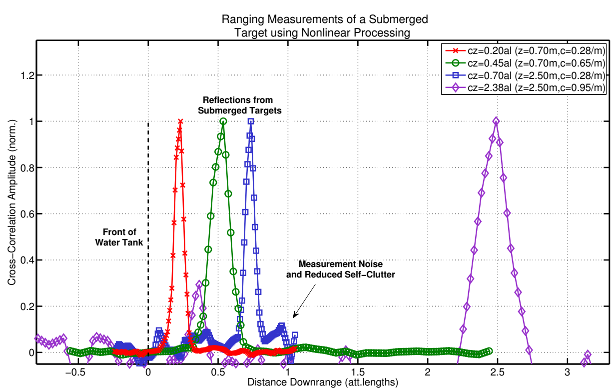

Fig. 17. When a nonlinear average mutual information processor is used to process the returns from Figure 15, the self-clutter artifacts from the transmitter are eliminated, and only measurement noise and the artifacts due to the receivers remain.

just downrange from, the main target peak. (These effects are consistent with those seen in previous lidar measurements, such as those in Figures 7 and 11, because they arise directly from the sensor hardware.) These artifacts are significantly reduced in the calibrated measurements, where no consistent self-clutter structures are seen, but only random measurement noise. The range resolution of the returns is also enhanced somewhat, because the smearing effect of the slowly rising main peak in the noise-like signal's autocorrelation has been removed, resulting in narrowed target peaks.

Nonlinear processing can also be used to reduce self-clutter due to non-ideal sensor hardware. The stochastic noise-like signals generated by the transmitter prototypes show high correlation dimensionality, and so their nonlinear auto-correlation can be more unique than their linear auto-correlation [21]. Therefore by substituting the average mutual information (AMI) nonlinear processor for the usual linear auto- and cross-correlation processing (i.e. the matched filter), self-clutter arising from the hardware can be suppressed. As with the calibration routine, the desired outcome is removal of self-clutter to allow operation in a noise-limited regime. Figure 17 shows the effect of using the AMI to process the measurements of Figure 15 instead of the cross-correlation. The linear cross-correlation measurements show several artifacts both from the autocorrelation of the transmitted signal, and from the receiver hardware. These artifacts are significantly reduced in the AMI-processed measurements, and the temporal resolution is again enhanced. However, some consistent structure seems to remain. Remaining self-clutter artifacts are thought to be due to the mismatch in receiver hardware, which is likely to involve primarily linear phenomena and therefore not to be affected by nonlinear processing. Thus the nonlinear processing has a similar self-clutter suppression effect to using a calibration routine, while not requiring additional calibration experiments. However, it may be insufficient if spurious receiver mismatch contributions are significant.

V. Conclusions

This paper introduces a new noise-like transmitter approach that generates wide bandwidth intensity modulation in the blue-green optical spectrum using low-cost, commercially available, compact components. Prototype transmitters have been demonstrated at multiple wavelengths, and power scaling using multiple diodes has been shown. Using a prototype transmitter, laboratory water tank measurements have shown that this transmitter approach can provide high range resolution impulse response and rangefinding measurements in a variety of water conditions. Several challenges have been identified in the experimental results: shot noise, backscatter peaks, and self-clutter. Several mitigation strategies have been proposed that are compatible with this wide bandwidth, nonlinear transmitter approach. These include modulation depth enhancement to increase the signal-to-shot-noise-ratio, frequency domain filtering to suppress backscatter peaks, and a calibration routine and nonlinear processing to decrease self-clutter. Future work will include improvement of modulation depth in the prototype transmitters, and rangefinding at extended operating ranges using the demonstrated processing techniques.

Acknowledgements

The authors thank Dr. Linda Mullen for use of the laboratory test tank facilities, and Alan Laux for his assistance with the experimental setup. This project is supported by the Office of Naval Research on grant #N000141410358.

References

[1] J.S. Jaffe, K.D. Moore, J. McLean, and M.P. Strand. Underwater optical imaging: status and prospects. *Oceanography*, 14(3):66–76, 2001.

[2] D.M. Kocak, F.R. Dalgleish, F.M. Caimi, and Y.Y. Schechner. A focus on recent developments and trends in underwater imaging. *Marine Technology Society Journal*, 42(1):52–67, 2008.

[3] F.R. Dalgleish, A.K. Vuorenkoski, and B. Ouyang. Extended-range undersea laser imaging: Current research status and a glimpse at future technologies. *Marine Technology Society Journal*, 47(5):128–147, 2013.

[4] J.S. Jaffe. Underwater optical imaging: The past, the present, and the prospects. *Oceanic Engineering, IEEE Journal of*, PP(99):1–18, 2014.

[5] T.J. Petzold. Volume scattering functions for selected ocean waters. Technical report, DTIC Document, 1972.

[6] E.P. Zege, A.P. Ivanov, and I.L. Katsev. *Image transfer through a scattering medium*. Springer Verlag, 1991.

[7] C.D. Mobley. *Light and water: Radiative transfer in natural waters*. Academic press, 1994.

[8] L.J. Mullen, A.J.C. Vieira, P.R. Herezfeld, and V.M. Contarino. Application of RADAR technology to aerial LIDAR systems for enhancement of shallow underwater target detection. *Microwave Theory and Techniques, IEEE Transactions on*, 43(9):2370–2377, 1995.

[9] F. Pellen, X. Intes, P. Olivard, Y. Guern, J. Cariou, and J. Lotrian. Determination of sea-water cut-off frequency by backscattering transfer function measurement. *Journal of Physics D: Applied Physics*, 33(4):349, 2000.

[10] J.W. McLean. High-resolution 3D underwater imaging. In *SPIE's International Symposium on Optical Science, Engineering, and Instrumentation*, pages 10–19. International Society for Optics and Photonics, 1999.

[11] F.R. Dalgleish, F.M. Caimi, W.B. Britton, and C.F. Andren. An auv-deployable pulsed laser line scan (PLLS) imaging sensor. In *OCEANS 2007*, pages 1–5. IEEE, 2007.

[12] B. Cochenour, L. Mullen, and J. Muth. Modulated pulse laser with pseudorandom coding capabilities for underwater ranging, detection, and imaging. *Applied Optics*, 50(33):6168–6178, 2011.

[13] L.K. Rumbaugh, M.K. Banavar, and W.D. Jemison. Underwater optical impulse response measurement using a chaotic lidar sensor. In *SPIE Defense Sensing and Security*, page 9459. International Society for Optics and Photonics, 2015.

[14] R.M. Narayanan, Y. Xu, P.D. Hoffmeyer, and J.O. Curtis. Design, performance, and applications of a coherent ultra-wideband random noise radar. *Optical Engineering*, 37(6):1855–1869, 1998.

[15] F.Y. Lin and J.M. Liu. Chaotic lidar. *Selected Topics in Quantum Electronics, IEEE Journal of*, 10(5):991–997, 2004.

[16] Y.C. Wang, B.J. Wang, and A.B. Wang. Chaotic correlation optical time domain reflectometer utilizing laser diode. *IEEE Photon. Technol. Lett*, 20(19):1636–1638, 2008.

[17] L.K. Rumbaugh, E.M. Bollt, Y. Li, and W.D. Jemison. A 532 nm chaotic lidar transmitter for high resolution underwater ranging and imaging. In *IEEE Oceans - San Diego, 2013*, pages 1–6, Sept 2013.

[18] J.S. Jaffe. Development of a laser line scan LIDAR imaging system for AUV use. Technical report, Scripps Inst. of Oceanography, Sept 2011.

[19] S. O'Connor, L.J. Mullen, and B. Cochenour. Underwater modulated pulse laser imaging system. *Optical Engineering*, 53(5):51403, 2014.

[20] D.W. Illig, L.K. Rumbaugh, M.K. Banavar, E.M. Bollt, and W.D. Jemison. Backscatter suppression via blind signal separation for a 532 nm underwater chaotic lidar rangefinder. In *IEEE Oceans - Washington, 2015*, Oct 2015.

[21] H. Kantz and T. Schreiber. *Nonlinear time series analysis*, volume 7. Cambridge University Press, 2004.

[22] H. Ludvigsen, M. Tossavainen, and M. Kaivola. Laser linewidth measurements using self-homodyne detection with short delay. *Optics Communications*, 155(1):180–186, 1998.

[23] M. Terrel, M.J.F. Digonnet, and S. Fan. Ring-coupled Mach-Zehnder interferometer optimized for sensing. *Applied Optics*, 48(26):4874–4879, 2009.

[24] M. Tur, B. Moslehi, and J.W. Goodman. Theory of laser phase noise in recirculating fiber-optic delay lines. *Lightwave Technology, Journal of*, 3(1):20–31, 1985.

[25] C. Pulikkaseril, E.H.W. Chan, and R.A. Minasian. Coherence-free microwave photonic bandpass filter using a frequency-shifting recirculating delay line. *Lightwave Technology, Journal of*, 28(3):262–269, 2010.